Effect of the Medium on Intramolecular H-Atom Tunneling: Cis−Trans Conversion of Formic Acid in Solid Matrixes of Noble Gases

Leonid I. Trakhtenberg,*,†,‡ Anatoly A. Fokeyev,‡ Alexander S. Zyubin,§ Alexander M. Mebel,*,‖ and S. H. Lin⊥

Semenov Institute of Chemical Physics, Russian Academy of Sciences, 4, Kosygina Str., Moscow 119991, Russia, SSC RF "Karpov Institute of Physical Chemistry", 10, Vorontsovo Pole Str., Moscow 105064, Russia, Institute of Problems of Chemical Physics, Russian Academy of Sciences, Chernogolovka, Moscow Region 142432, Russia, Department of Chemistry and Biochemistry, Florida International University, Miami, Florida 33199, United States, and Department of Applied Chemistry and Institute of Molecular Sciences, National Chiao-Tung University, Hsin-chu 10764, Taiwan

Intramolecular tunneling of a hydrogen atom in formic acid at low temperatures has been studied theoretically on the basis of quantum-chemical modeling of HCOOH@Nb$_{12}$ clusters. Three noble matrixes (Ar, Kr, and Xe) are considered. Energetic and geometric parameters as well as vibrational frequencies for the formic acid in cis and trans configurations surrounded by 12 Nb atoms are calculated within the frame of the MP2 approach with extended basis sets. The rate constant of HCOOH cis−trans conversion is analyzed by taking into account matrix reorganization and the change of HCOOH position in the cluster. The matrix reorganization is considered within the Debye model of lattice vibrations, whereas the external motion of HCOOH in the cluster is treated using the Einstein model of solids. It has been shown that the literature experimental data on the cis to trans tunneling reaction in the formic acid can be accounted for within the proposed mechanism, which describes the matrix reorganization and the change of the HCOOH position in the noble gas matrix, with fitting parameters of the suggested theoretical model attaining reasonable values.

I. Introduction

It is known that the tunneling mechanism of atomic transfer plays the critical role in reaction kinetics at very low temperatures. The medium has a strong effect on the tunneling processes.[1−3] This effect appears in the temperature and pressure dependence of the tunneling rate constant (see, for example, refs 1−5 and references here). The origin of this dependence in many respects is determined by the reaction type. In the case of chemical reactions involving an intermolecular H-atom transfer,[6−11] the most important mechanisms responsible for the temperature effects include an amplitude change of intermolecular vibrations (promotive modes)[6−10] and reorganization of the medium.[11] The medium reorganization energy was first introduced in chemical kinetics for classical vibrations of the medium.[12] Then, the rate constants accounting for the medium reorganization mechanism were determined for the quantum case within the Einstein model of vibrations of surrounding molecules,[13,14] and recently also in a continuous phonon spectrum.[15,16] Meanwhile, as follows from the Debye model of solids, a truly continuous spectrum is justified only at very low temperatures. A theoretical approach for the mechanism of temperature dependence of the tunneling rate constant originated from the influence of intermolecular vibrations on the potential barrier to be overcome by the tunneling particle was first

proposed in 1978[17] and was further developed in later works.[1,2,15,16,18−20] Numerous examples that compare theoretical results of these two models with experimental data are given in these publications.

Several extensive surveys of numerous experimental results can be found in the literature concerning the reactions involving intramolecular H-atom tunneling.[21,22] Usually, a tunneling process occurs in very complicated molecular systems, so that a rigorous consideration of the medium effects is not a simple task. Solid noble gases represent the simplest matrixes, and temperature-dependent tunneling rate constants were recently measured for the cis−trans isomerization of the formic acid molecule in solid Ar, Kr, and Xe at extra low temperatures.[23,24] In these experiments, HCOOH is excited from the ground trans state to the higher-energy cis conformer. Then, a spontaneous reverse cis−trans process takes place via H-atom tunneling. The studies of chemical reactions of organic compounds in matrixes of solid noble gases have begun several decades ago,[25,26] and various mechanisms of chemical transformations of simple molecules in inert matrixes have been explored experimentally since then.[27−29,23,24]

The tunneling mechanism was first confirmed for intramolecular reactions by Brunton et al.[30,31] They investigated isomerization of aryl radicals in hydrocarbon solvents in a wide temperature range of 28−240 K, and the low temperature limit of the rate constant was observed near 100 K. For the reactions in the noble gas matrixes, very detailed data on the temperature dependence of tunneling rate constants of the intramolecular H-atom transfer in the formic acid in different inert matrixes are available.[23,24] It should be emphasized that a matrix is "inert" only in the sense that it does not affect the result of chemical transformation, but as shown experimentally,[23,24] the temperature

* Corresponding author. E-mail: L.I.T., trakh@cc.nifhi.ac.ru; A.M.M, mebela@fiu.edu.
† Semenov Institute of Chemical Physics, Russian Academy of Sciences.
‡ SSC RF "Karpov Institute of Physical Chemistry".
§ Institute of Problems of Chemical Physics, Russian Academy of Sciences.
‖ Florida International University.
⊥ National Chiao-Tung University.

Cis−Trans Conversion of Formic Acid in Noble Gases

J. Phys. Chem. B, Vol. 114, No. 51, 2010 **17103**

dependence of the reaction kinetics strongly depends on the type of the noble gas involved.

One can imagine various mechanisms, which can be responsible for the medium influence on the intramolecular tunneling process, including a change of the barrier height and shape due to the reagent interaction with surrounding molecules and matrix reorganization. These mechanisms were proposed earlier[32,33] for different monomolecular reactions, and the appropriate theoretical approach to describe them was developed in these works and some experimental data were discussed.[33] The aforementioned mechanisms pertinent to the media influence on the formic acid conversion inside an Ar_{12} model cluster were investigated in our recent papers.[34,35] It has been shown that the matrix reorganization upon the intramolecular H-atom transfer described within the Debye model of lattice motion plays the key role in the temperature dependence of the rate constant. One of the purposes of the present work is to investigate the effect of heavier rare gas matrixes on the barrier of the HCOOH cis−trans conversion and to evaluate reorganization effects in this process by means of quantum chemical modeling (sections 2−4). Note that an adequate theoretical description of the HCOOH−Nb interaction (where Nb stands for a noble gas atom) requires the use of high-level approaches, which take electron correlation effects into account. Previously, such high-level calculations were only reported for HCOOH-Ar[36] and HCOOH@Ar_{12}.[34,35]

The present work is devoted to quantum chemical calculations of the HCOOH molecule inside the first coordination sphere of solid Nb atomic matrixes in the Ar−Kr−Xe row. It seems that such a cluster model should be sufficient to reproduce main features of matrix effects on the tunneling process during the HCOOH cis−trans conversion. The most important mechanism of the matrix influence is expected to be the following. It is known that this molecule changes its configuration upon H-atom transition, and the matrix geometry adjusts accordingly, which leads to an appearance of the reorganization energy of the system.[34,35] As a result, the H-atom tunneling rate constant depends on temperature. For the rate constant calculations, it is also necessary to take into account the fact that some frequencies of HCOOH librations and rotations in the Nb_{12} cluster are comparable with the Debye frequency ω_D, especially for the heavier Xe matrix. Therefore, an analytical expression for the tunneling rate constant should take care of not only the matrix reorganization but also HCOOH motions inside the Nb_{12} cluster (section 5). The derived expression is compared with experimental data[23,24] in section 6.

2. Calculation Details

Solid noble gases possess a cubic close-packed crystal structure[37−39] with 12 neighbors surrounding each atom (Figure 1). Since the sizes of the formic acid molecule and Ar, Kr, and Xe atoms do not differ significantly, embedding the HCOOH molecule in a condensed Nb gas matrix occurs in place of one of the Nb atoms, having 12 neighbors in the first surrounding layer. Such system can be considered as minimal to simulate the HCOOH-Nb matrix interaction. As the Nb−Nb and Nb−HCOOH interactions are determined mainly by dispersion effects, an account of electron correlation (at the MP2, MP4, or CCSD levels of theory with flexible basis sets containing polarization and diffuse functions) is required for its appropriate description. It was demonstrated earlier[34,35] that the MP2 approach (Möller−Plesset perturbation theory up to the second order) with basis sets including diffuse and polarization functions is suitable for this purpose. The calculations were performed here using the GAUSSIAN 03[40] program package.
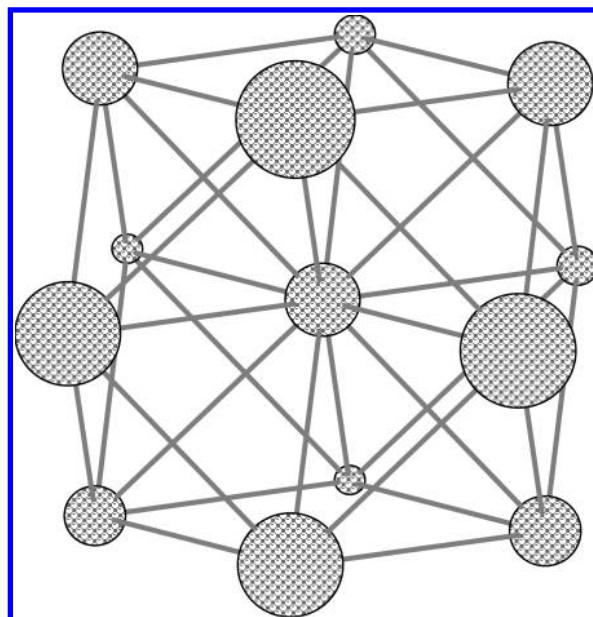

Figure 1. Fragment of a noble gas crystal.

TABLE 1: Nb−Nb Interaction Parameters Calculated with Different Basis Sets, Including *R*, the Inter-atomic Distance (Å), *D*$_e$, the Interaction Energy (cm^{-1}), and BSSE, the Basis Set Superposition Error (cm^{-1})

system	method	R (Å)	D_e (cm^{-1})	BSSE	D_e(BSSE)
Ar_2	MP2/PVTZ	4.0	52		
	MP4/PVTZ	4.05	38		
	MP2/LanL2apDZ	3.8	182	168	14
	MP4/LanL2apDZ	3.75	210	192	18
	MP2/APVDZ	3.95	87	35	52
	MP4/APVDZ	4.0	77	38	39
	MP2/APVTZ	3.8	112	28	84
	MP4/APVTZ	3.8	98	24	74
	exp	**3.72**	**52**		
Kr_2	MP2/CEP-31ap	4.13	140	98	42
	MP4/CEP-31ap	4.15	136	105	31
	MP2/LanL2apDZ	4.05	245	203	42
	MP4/LanL2apDZ	4.06	259	227	32
	MP2/SDDa	4.11	136	42	94
	MP4/SDDa	4.18	112	42	70
	MP2/SDDa′		84	28	56
	MP4/SDDa′		42	28	14
	MP2/APVDZ	4.12	147	87	60
	MP4/APVDZ	4.20	122	91	31
	MP2/APVTZ	3.96	241	122	119
	MP4/APVTZ	4.01	210	119	91
	exp	**4.04**	**73**		
Xe_2	MP2/CEP-31ap	4.59	171	115	55
	MP4/CEP-31ap	4.57	147	133	14
	MP2/LanL2apDZ	4.55	213	171	42
	MP4/LanL2apDZ	4.61	189	147	34
	MP2/SDDa	4.48	192	63	129
	MP4/SDDa	4.57	150	70	80
	MP2/SDDa′		119	59	60
	MP4/SDDa′		66	66	0
	exp	**4.42**	**105**		

A potential energy scan along the Nb−Nb distance in the Nb_2 diatomic complex shows that the results of the MP2 and MP4 calculations are similar (Table 1), and hence the simpler MP2 is adequate for modeling the Nb−Nb interactions. Calculations with the extended aug-cc-pVTZ basis set[40−42] (triple-ζ augmented by diffuse and polarization functions, APVTZ in short) give the minimum energy positions of the Ar_2 and Kr_2 potential energy curves close to the corresponding

experimental values, but the interaction energies are overestimated (Table 1). Taking the basis set superposition error (BSSE) into account improves the agreement between the calculated and experimental interaction energies. A removal of diffuse functions from the basis set in use (PVTZ) results in a substantial underestimation of the Nb−Nb interaction. A simpler double-ζ aug-cc-pVDZ (APVDZ) basis set, which includes diffuse functions, provides more reasonable results (Table 1). But even APVDZ is too cumbersome for the model system under investigation. One can simplify the calculations by replacing core electrons with a pseudopotential with a suitable core-less basis set. Hence, we tested the LanL2 pseudopotential[40,43−45] with the corresponding double-ζ basis set augmented by diffuse and polarization functions taken from aug-cc-pVDZ (LanL2apDZ). This approach reproduces the minimum energy positions reasonably well, but the Nb−Nb interaction energies are substantially overestimated in direct calculations and are underestimated with the BSSE correction included (Table 1). Therefore, one can use the MP2/LanL2apDZ approach for geometry optimization, but the energy values should be refined with more flexible basis sets. Additionally, the MP2/LanL2apDZ approach was tested for the Ar_{13} model system (Figure 1). In this case, the calculated Ar−Ar distance between central atom and its neighbors was 3.706 Å, in good agreement with the experimental value for solid Ar, 3.717 Å.[37]

For the heavier Nb atoms, Kr and Xe, we additionally tested other pseudopotentials available in GAUSSIAN 03, including SBK[46−48] with the CEP-31 basis set and the more flexible but also more computationally demanding SDD[40,49−53] pseudopotential with the corresponding (3111s/3111p/111d/1f) basis set including polarization functions. CEP-31 was augmented by polarization and diffuse functions (CEP-31ap), whereas for SDD we added diffuse functions only (SDDa). Exponential factors for these functions were taken from aug-cc-pVDZ, but since this basis set is not available for Xe, its exponents were extrapolated in the Ar−Kr−Xe row. In addition, we tested a simplified SDDa′ basis set, which does not include f-functions. The calculation results with the CEP-31ap basis set are slightly worse in comparison with those obtained using LanL2apDZ. Calculations with the SDDa basis set do not lead to significant refinement of Nb−Nb distances, but the description of interaction energies is much better than with LanL2apDZ and CEP-31ap. The use of the reduced SDDa′ basis set leads to underestimation of the interaction energies with the BSSE correction, but the energy values without this correction are reasonable.

At the next stage, we tested the performance of the selected theoretical approaches for the description of the Nb−HCOOH interaction. The calculated results for Ar−HCOOH[36] were taken as the reference data. In the most stable form of this complex, the Nb atom is located approximately along the O−H bond (Figure 2). Geometry optimization for this configuration was performed at the MP2 level with the B2 basis set, including APVDZ for O, C, H and LanL2DZap for Nb. The Nb−HCOOH interaction energy was refined with more flexible basis sets at the optimized structures. Optimization at the MP2/B2 level for Nb = Ar leads to approximately the same structure of the complex as that obtained in the previous work,[36] but with a slightly shorter Ar−H distance (Table 2). For heavier Nb atoms, this value grows in a similar proportion as R(Nb−Nb) (Tables 1 and 2). The Nb−HCOOH interaction energies (D_e) calculated at the MP2/B2 level without BSSE are overestimated, but the BSSE corrected values are too low. Moreover, at this level of theory the D_e behavior is nonmonotonous in the Ar−Kr−Xe
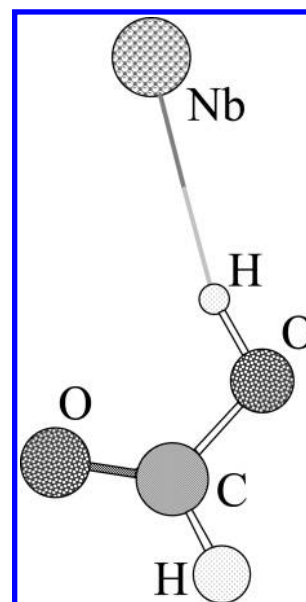

Figure 2. Nb−HCOOH (trans) complex.

TABLE 2: Nb−HCOOH Interaction Parameters Calculated with Different Basis Sets[a]

basis set	R(H−Nb), Å	D_e (cm^{-1})	BSSE	D_e(BSSE)
Ar				
MP2/B2	2.55	633	559	73
MP2/B3	2.55*	468	336	132
MP2 [a]	2.63			133
MP4 [a]				84
Kr				
MP2/B2	2.63	806	794	12
MP4/B2		902	882	20
MP2/SDDa′d		311	192	119
MP4/SDDa′d		332	222	110
MP2/SDDad		325	180	145
MP4/SDDad		338	199	139
MP2/B3		775	618	157
MP2/SDDa′t		517	318	199
MP2/SDDat		453	236	217
MP2/APVTZ		597	377	220
Xe				
MP2/B2	2.82	748	686	62
MP4/B2		846	780	66
MP2/SDDa′d		388	229	159
MP4/SDDa′d		395	287	108
MP2/SDDad		403	206	197
MP4/SDDad		421	235	186
MP2/SDDa′t		638	392	246
MP2/SDDat		588	313	275

[a] D_e is the interaction energy (cm^{-1}). BSSE is the basis set superposition error (cm^{-1}). The basis set notation is as follows. B2: Nb, LanL2DZap; O, C, H, APVDZ. B3: Nb, APVDZ; O, C, H, APVTZ; SDDad, SDDa′d: O, C, H, APVDZ, and SDDa and SDDa′ at Nb. SDDat, SDDa′t: O, C, H, APVTZ, and SDDa and SDDa′ at Nb.

row. With fuller and more flexible APVTZ, SDDat, and SDDa′t (SDDa and SDDa′ at Nb and APVTZ at O, C, H) basis sets the results are more reasonable; the interaction energy grows in the Ar−Kr−Xe row. As for the Nb−Nb interaction, there is no substantial difference between the MP2 and MP4 results, and the basis set quality seems to be similar for SDDat and APVTZ; moreover, the D_e values with the reduced SDDa′ basis set deviate by only ∼10% from the SDDat data (Table 2). On the basis of these results, one can conclude that the MP2/B2 level is suitable for geometry optimization for the systems under
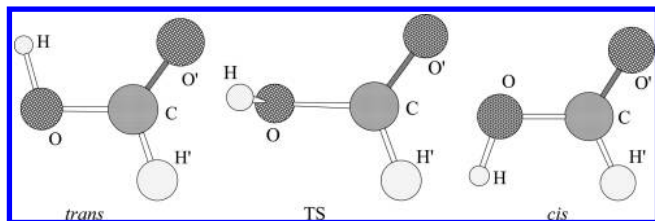
Cis—Trans Conversion of Formic Acid in Noble Gases

J. Phys. Chem. B, Vol. 114, No. 51, 2010 **17105**

Figure 3. Formic acid in trans, TS, and cis configurations.

Figure 4. Optimized C configurations of the Nb_{12}@HCOOH system (cis and trans isomers). X is the center of the system.

investigation, but the energy values should be refined with fuller and more flexible APVTZ, SDDat, or SDDa′t basis sets. It is worth noting that the BSSE correction is significant when one considers separation of the system, when basis set functions from one fragment are unable to contribute to the wave function of the counter-fragment and vice versa. However, for intramolecular rearrangements, such as, for instance, internal rotation, the mutual contributions of basis sets from different parts of the system are similar for different configurations, and the BSSE correction has only a weak effect on their relative energies.

Finally, the selected theoretical approach needs to be tested for the description of molecular properties of HCOOH. The global minimum of this molecule corresponds to the trans isomer. By means of the OH group rotation around the C—O axis, the molecule passes through a transition state (TS) to the cis isomer (Figure 3) with a higher energy (local minimum). For testing purposes both isomers of this molecule and the transition state (barrier) between them were calculated at the MP2/APVDZ and MP2/APVTZ levels. The calculated molecular properties (geometry parameters, vibrational frequencies, and relative energies) were found to be in good agreement with other high-level calculations and the experimental data available[36,54−56] (Tables 3 and 4). Moreover, there is no substantial difference between relative energies calculated with the APVDZ
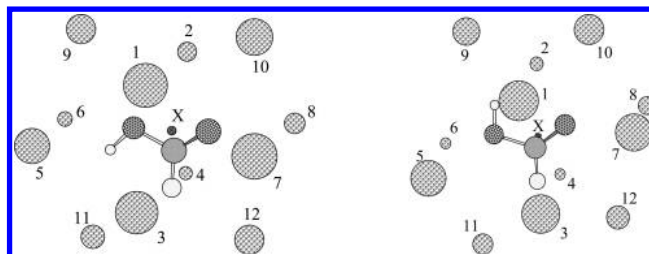
and APVTZ basis sets (Table 4). Thus, the levels of theory used in this work are suitable for describing the HCOOH cis—trans rearrangement.

3. Embedding HCOOH in the Cell of a Noble Gas Matrix

It was demonstrated earlier[34,35] that HCOOH has several orientations in Ar_{12} cage, but properties of the barrier for the cis—trans conversion are similar for all of these configurations. In this paper we used for the entire Ar—Kr—Xe row the most stable C_s-symmetric form C (Figure 4), where HCOOH is parallel to two of the cube faces.

Optimization of geometry parameters for the HCOOH@Nb_{12} systems leads to very weak variations of HCOOH bond lengths and valence angles as compared to those of the isolated molecule (Table 5). It is apparent from the available data that the matrix effects are somewhat higher for heavier Nb atoms, but the trend is not very clear. In contrast, Nb_{12} cages are significantly distorted due to the interaction with HCOOH. After geometry optimization, the Nb atoms located approximately in equatorial positions relative to the C—O bond (numbered as 1−4) are

TABLE 3: Optimized Geometry Parameters for Cis, Trans, and TS Forms of Formic Acid[a]

	R(CO)	R(CO′)	R(CH′)	R(OH)	φ(O′CO)	φ(H′CO)	φ(HOC)	τ(HOCO′)
				Trans				
MP2/B1	1.358	1.215	1.103	0.975	125.1	109.5	106.3	0.0
MP2/B2	1.347	1.205	1.092	0.971	125.1	109.7	106.5	0.0
MP2/B3[5]	1.348	1.204	1.090	0.967	125.1	109.8	106.8	0.0
CCSD/B4[23]	1.351	1.210	1.099	0.973	125.1	109.6	106.6	0.0
exp[23]	1.343	1.202	1.097	0.972	124.6	111.3	106.3	0.0
				TS				
MP2/B1	1.390	1.208	1.107	0.969	123.7	112.5	109.9	94.1
MP2/B2	1.377	1.197	1.096	0.965	123.7	112.5	110.4	94.3
				Cis				
MP2/B1	1.365	1.209	1.109	0.970	122.2	113.7	108.7	180.0
MP2/B2	1.354	1.199	1.099	0.966	122.3	113.5	108.9	180.0
MP2/B3[5]	1.355	1.197	1.096	0.962	122.4	113.5	108.9	180.0
CCSD/B4[23]	1.357	1.204	1.105	0.968	122.7	113.6	108.7	180.0
exp[23]	1.352	1.195	1.105	0.956	122.1	114.6	109.7	180.0

[a] The basis set notation is as follows. B1: AUG-cc-pVDZ. B2: AUG-cc-pVTZ. B3: 6-311++G(2d,2p). B4: DZp.

TABLE 4: Relative Energies E_r (cm^{-1}) and Zero-Point vibrational Energies (ZPE) for Trans, Cis, and TS Configurations of Formic Acid[a]

	trans	TS			cis		
	ZPE	Er	ZPE	Er+ZPE	Er	ZPE	Er+ZPE
MP2/B1	7388	4565	6928	4105	1492	7307	1403
MP2/B2	7436	4533	6985	4089	1484	7356	1403
MP2/B3[5]		4565			1492		
CCSD(T)/B4[23]	7695	4678	7307	4291	1565	7799	1460
exp[25]							1363

[a] The zero E_r value corresponds to the trans isomer.

TABLE 5: Optimized Geometry Parameters for Cis and Trans Forms of the Formic Acid in the Nb$_{12}$ Cell[a]

	R(CO)	R(CO′)	R(CH′)	R(OH)	Φ(O′CO)	φ(H′CO)	φ(HOC)	τ(HOCO′)
				Trans				
isolated	1.358	1.215	1.103	0.975	125.1	109.5	106.3	0.0
Ar	1.354	1.216	1.098	0.975	125.0	109.8	106.5	0.0
Kr	1.353	1.217	1.098	0.976	125.0	109.7	106.8	0.0
Xe	1.354	1.218	1.101	0.978	125.1	109.7	107.0	0.0
				Cis				
isolated	1.365	1.209	1.109	0.970	122.2	113.7	108.7	180.0
Ar	1.360	1.210	1.103	0.970	122.0	113.8	108.5	180.0
Kr	1.360	1.211	1.103	0.971	121.9	113.9	108.5	180.0
Xe	1.361	1.213	1.106	0.973	121.9	114.0	108.6	180.0

[a] The basis set notation is as follows. Nb: LanL2DZap. O, C, H: APVDZ.

TABLE 6

a. Distances from the Cluster Center to Nb Atoms ($R(X-Nb_k)$, Å) for Cis and Trans Isomers of HCOOH in the Nb$_{12}$ Model Cluster (Figure 4)

k	1, 2	3, 4	5, 6	7, 8	9	10	11	12
Ar, cis	3.16	3.52	4.21	3.94	3.97	3.82	4.03	3.88
Ar, trans	3.30	3.50	4.20	3.87	4.04	3.85	3.95	3.62
Kr, cis	3.40	3.62	4.22	4.20	4.15	4.18	3.95	3.99
Kr, trans	3.42	3.66	4.21	4.17	4.10	4.12	3.93	4.02
Xe, cis	3.69	3.95	4.48	4.43	4.42	4.46	4.19	4.27
Xe, trans	3.74	3.97	4.48	4.40	4.38	4.45	4.20	4.28

b. Displacements of Nb Atoms from Their Crystalline Positions ($S(Nb_k)$, Å) after Embedding of the Cis Isomer of HCOOH in the Nb$_{12}$ Model Cluster (Figure 5)

k	1, 2	3, 4	5, 6	7, 8	9	10	11	12
Ar	0.68	0.95	0.99	0.80	0.45	0.44	0.76	0.38
Kr	0.81	0.99	1.04	0.81	0.58	0.44	0.77	0.73
Xe	1.05	1.05	1.11	1.14	0.74	0.63	0.90	0.92

c. Displacements of Nb Atoms ($S(Nb_k)$, Å) in the Nb$_{12}$ Model Cluster after the Cis−Trans Conversion of HCOOH (Figure 4)

k	1, 2	3, 4	5, 6	7, 8	9	10	11	12
Ar	0.52	0.35	0.86	0.39	0.52	1.12	0.34	0.39
Kr	0.20	0.13	0.04	0.05	0.22	0.30	0.10	0.08
Xe	0.12	0.07	0.06	0.02	0.14	0.10	0.11	0.06

shifted toward the center of the system, whereas the other Nb atoms (5−12) are displaced in the opposite direction (Figure 4, Table 6). The displacements are sizable, up to 0.5−0.7 Å, mainly for the "equatorial" Nb atoms, which are attracted to the HCOOH molecule. In a real system, the distortion of the noble gas lattice by HCOOH would lead mainly to a compression of the first coordination shell around the impurity with gradual attenuation of deformations in the next layers. Thus, the deformation of the Nb$_{12}$ cage surrounding the impurity in the bulk should be smaller than in the present model due to attractive influence of the outer shells. Nevertheless, the main trends are expected to be similar because the Nb−HCOOH interactions are significantly stronger in comparison with the Nb−Nb interaction, as was shown earlier in the case of Ar.[35]

The vibrational analysis revealed one imaginary frequency of ∼3 cm^{-1} for the cis isomer of HCOOH in the Ar$_{12}$ cluster. Reoptimization of this configuration along coordinates corresponding to this vibration has led to approximately the same structure but with C_1 symmetry. There were no imaginary frequencies in this configuration, but the energy decrease was negligibly small (∼0.6 cm^{-1}). A probable reason of this result could be round-up errors in integral calculations, and for further investigations we used the configuration with C_s symmetry. For the Kr and Xe cages, the optimized C_s-symmetric configurations have no imaginary frequencies.

For all HCOOH@Nb$_{12}$ systems, calculated frequencies can be clearly separated into three groups, internal vibrations of HCOOH (with slight variations from the corresponding values

in the isolated molecule), six vibrations of HCOOH as a rigid particle in the Nb$_{12}$ cell (with values from 200 to 60 cm^{-1}), and vibrations of the Nb atoms from the Nb$_{12}$ shell, which cover the range from 60−40 cm^{-1} to almost zero (Table 7). The frequency values from the second and the third groups have a clear tendency to decrease in the Ar−Kr−Xe row, but the reasons for such a behavior are different. In the third group the main reason of the decrease is the increase of the atomic mass of Nb, whereas for the second group the main factor is the reduction of the corresponding force constants. This means that the interaction potential between HCOOH and the Nb$_{12}$ cage is smoother for heavier atoms.

4. Mutual Influence of Nb$_{12}$ and HCOOH on Their Energetic and Geometric Characteristics

Tunneling proceeds adiabatically - while the H atom penetrates the potential barrier, the other atoms remain at the initial or final position corresponding to the minimal energy of the respective conformation of HCOOH@Nb$_{12}$. Such consideration is commonly called in the literature as a double adiabatic approximation.[1,14,15] The reaction system chooses the configuration in which the tunneling takes place. It may be the initial or final state, subject to the proper value of the potential barrier. It is clear that tunneling is more probable when the barrier is smaller. For example, the intermolecular transfer of hydrogen atom in fluorene−acridine system occurs in the final configuration of reagents, where the potential barrier is significantly

TABLE 7: Vibrational Frequencies (cm⁻¹) of the Cis and Trans Isomers of the Formic Acid in the Nb_{12} Clusters

assignment	isolated	Ar		Kr		Xe		isolated	Ar		Kr		Xe	
		trans							*cis*					
O−H str	3728 A′	3721		3705		3675		3790	3791		3766		3738	
C−H str	3138 A′	3193		3187		3154		3052	3111		3121		3090	
C=O str	1772 A′	1775		1768		1758		1805	1805		1798		1788	
HCO bend.	1396 A′	1411		1406		1397		1404	1422		1418		1407	
HOC bend.	1295 A′	1305		1303		1297		1274	1278		1273		1267	
C−O str	1116 A′	1124		1122		1116		1097	1120		1118		1110	
HCOO tors	1047 A″	1068		1066		1060		1020	1032		1030		1026	
HOCO tors	673 A″	683		671		672		525	527		522		512	
OCO bend.	618 A′	624		624		621		643	649		647		644	
HCOOH		202		205		172			220		212		170	
librations		118		116		96			126		115		92	
and		116		109		88			114		105		86	
rotations		105		98		79			110		101		81	
in the Nb_{12}		103		97		77			108		101		73	
cluster		90		80		64			94		80		59	
		62	61	45	44	39	39		62	620	44	43	38	38
		59	58	43	43	34	34		60	59	43	43	34	34
		56	54	41	41	33	32		57	55	42	39	33	33
		53	51	37	337	32	30		48	48	38	35	32	30
vibrations		48	44	34	33	30	29		43	43	33	32	30	30
of the Nb_{12}		43	41	32	31	29	26		42	39	32	31	29	27
cluster		38	36	30	28	26	24		36	35	30	28	26	26
		36	35	27	26	23	23		34	33	28	27	24	23
		31	31	24	23	22	21		32	31	26	25	23	21
		29	29	22	21	20	20		30	29	24	23	20	20
		28	25	20	19	20	19		26	26	22	22	19	19
		24	24	19	17	18	16		24	22	20	19	18	17
		21	20	17	17	16	16		22	18	17	17	16	15
		17	15	16	14	15	15		15	15	17	13	15	15
		12	9	13	9	12	9		8	3i	7	6	11	5

TABLE 8: Adiabatic Energy Profiles (cm⁻¹) for the HCOOH Cis−Trans Conversion[a]

τ	isolated cis	isolated trans	Ar_{12} cis	Ar_{12} trans	Kr_{12} cis	Kr_{12} trans	Xe_{12}t cis	Xe_{12} trans
180	0	0	0	0	0	0	0	0
165	198	198	195	187	196	219	166	180
150	751	753	729	689	741	803	676	711
135	1536	1543	1487	1373	1524	1598	1464	1502
120	2350	2364	2319	2120	2377	2427	2314	2349
105	2956	2961	3012	2775	3061	3064	2982	3009
90	3138	3103	3287	3031	3313	3261	3230	3229
75	2794	2682	2970	2662	2987	2870	2903	2855
60	1982	1762	2146	1752	2162	1959	2073	1964
45	907	569	1075	572	1093	781	973	779
30	−152	−597	25	−602	64	−364	−85	−399
15	−919	−1437	−745	−1497	−671	−1194	−793	−1222
0	−1201	−1742	−1029	−1840	−933	−1493	−1009	−1482
σ	45.70	43.25	47.06	43.14	47.65	46.40	46.15	45.51

[a] Zero energy corresponds to the cis configuration. τ denotes the torsional HOCO′ angle in degrees. The basis set notation is as follows. Ar: LanL2DZap. Kr: SDDa. Xe: SDDa′. O, C, H: APVTZ.

lower.[5,16,34] In the given system the barrier was calculated for the initial and final configurations. It turned out to be close in value and shape for both cases (Table 8). The scan of the potential energy profile for the HCOOH cis−trans conversion in the Ar−Kr−Xe matrixes was carried out with geometry parameters optimized for the cis and trans isomers. The exponential factor for a quasiclassical tunneling process was calculated for each profile as

$$\sigma(l) = 2 \int \{2m_H[U(x) − E_H]\}^{1/2} \, dx \qquad (1)$$

where $U(x)$ is the potential barrier height at the point x and m_H and E_H are the mass and the energy of the tunneling H-atom.

Integration was carried out along the arc l of the H motion for the region with $U(x) > E_H$. All values are in atomic units.

The results of potential energy scanning show only a weak influence of the Nb_{12} cluster on the barrier parameters (Table 8). In the Ar_{12} cage (Figure 4C) both barrier height and σ value are only several percent different from those for the isolated molecule of the formic acid. For HCOOH in the Kr and Xe clusters, variations of the barrier height and σ values are small and nonmonotonous. According to the data in Table 5, variations of the basis set (AUG-cc-pVDZ or AUG-cc-pVTZ) cause a barrier height change of ~0.4% and the corresponding change of the σ value turns out to be ~0.1. Taking into account that the σ value is in the ~40−50 range, this error, since it is in the exponent, dramatically affects the accuracy of the calculated

TABLE 9: Reorganization Energies (cm^{-1}) and Their Components in the HCOOH@Nb$_{12}$ Cluster (Trans) after Tunneling from the Cis Form, Configuration C^a

	Ar, b1	Kr, b1	Xe, b1	Ar, b2	Kr, b4	Xe, b4	Ar, b2*	Kr, b4*	Xe, b4*
full (Nb$_{12}$ + FA)	396	367	326	353	322	297	364	334	350
FA-inner	272	269	270	249	246	253	263	263	268
Nb$_{12}$ and FA position	124	98	56	104	76	44	101	71	82
FA position (E$_r'$)	62	68	41	64	63	25	58	56	31
Nb$_{12}$ only (E$_r$)	62	30	15	40	13	19	43	15	51
RE	1376	1295	1262	1373	1226	1190	1334	1230	1202

^{a} FA denotes formic acid. Released energy (RE) is the energy difference between the cis and trans isomers in the ground states. The basis set notation is as follows. b1: LanL2apDZ at Ar, Kr, Xe; aug-cc-pVDZ at O, C, H. b2: aug-cc-pVDZ at Ar; aug-cc-pVTZ at O, C, H. b4: SDDa′ at Kr or Xe; aug-cc-pVTZ at O, C, H. Asterisks (*) designate BSEE-corrected energies.

absolute magnitude of the tunneling rate constant. However, as will be shown in section 6, these absolute magnitudes are not essential for the comparison of the theoretical and experimental temperature dependences of the rate constant.

From our previous results, we can see that the interaction energy between the Nb atom and HCOOH molecule grows in the Ar−Kr−Xe row (Table 2), but the potential energy for HCOOH in the Nb$_{12}$ cage becomes smoother in the same row (see HCOOH librations and rotations in Table 7). Apparently, these two factors affect the barrier profile in opposite directions resulting in a nonmonotonous behavior of the barrier height and σ values.

It was demonstrated earlier[34,35] that the temperature dependence of the HCOOH cis−trans conversion rate constant in a noble gas matrix does not originate from a change in the potential barrier due to the matrix vibrations but is rather caused by reorganization processes in the reaction system. Therefore, in this work we estimated different components of the reorganization energy associated with the H penetration through the potential barrier. To do so, we calculated energies of the following structures:

1. The trans isomer of HCOOH@Nb$_{12}$ with all geometry parameters taken from the cis configuration, except for the HOCO dihedral angle.

2. For the configuration taken from step 1, all internal parameters (interatomic distances and bond angles) of the HCOOH molecule were optimized, but its position in the Nb$_{12}$ cluster and coordinates of the Nb atoms were frozen.

3. The HCOOH position in the cluster was also optimized.

4. Coordinates of all Nb atoms were optimized (full optimization).

Using differences of the energies calculated at these four steps, one can evaluate the energy components related only to the reorganization of Nb atoms (denoted as Nb$_{12}$ only), reorientation of HCOOH in the cluster (FA position) and relaxation of the HCOOH bonds and bond angles (FA-inner). Geometry optimization was carried out at the MP2 level with the basis sets LanL2apDZ at Ar, Kr, and Xe, aug-cc-pVDZ at O, C, and H; the energies were then refined with the more flexible basis sets aug-cc-pVTZ at O, C, and H, aug-cc-pVDZ at Ar, and SDDa′ at Kr or Xe. The calculated components of the reorganization energy and the energy difference between the optimized cis and trans isomers (denoted as EDCT) are presented in the Table 9.

It follows from these results that the EDCT value for HCOOH@Nb$_{12}$ is smaller than that for isolated HCOOH (1484 cm^{-1} at the MP2/B2 level) and decreases in the Ar−Kr−Xe row with all the basis sets used and taking BSSE into account (Tables 4 and 9). Obviously, the interaction of the cis isomer with the Nb$_{12}$ cluster is stronger as compared to the trans isomer interaction, and for heavier Nb atoms the difference is more

substantial. In contrast, the barrier height for the OH group rotation remains almost unchanged in this row. The total reorganization energy is ∼300−400 cm^{-1}, and the main contribution is the FA-inner energy corresponding to the reorganization of HCOOH bond angles and distances. Its value is almost unchanged in the Ar−Kr−Xe row, and the basis set dependence is also weak (Table 9). The energy decrease due to the reorientation of HCOOH in the cluster (FA position) is approximately equal in the Ar and Kr clusters, but it is significantly lower for Xe, with all basis sets (Table 9). The reorganization energy of the Nb$_{12}$ cluster (Nb$_{12}$ only) is the largest for Ar and much lower for Kr and Xe. For this quantity, the basis set dependence appears to be significant. Because the b2 and b4 basis sets are more suitable for the description of the Nb−Nb interaction as compared to b1, the values calculated with these basis sets seem more reliable. The account of BSSE does not change this energy for Ar$_{12}$ and Kr$_{12}$, but for Xe$_{12}$ the value with BSSE is much higher (Table 9). Possibly, this is a result of insufficiently accurate evaluation of integrals involving diffuse functions with high angular momenta when the functions are located away from the nuclei as in the calculations of counterpoise corrections for BSSE, and hence the results without BSSE are preferable.

5. Temperature Dependence of the Rate Constant of Intramolecular Hydrogen Tunneling

Quantum-chemical calculations described above show that the main variations occurring upon intramolecular H-atom tunneling concern the positions of the atoms in the reaction system, HCOOH@Nb$_{12}$. This leads to changes of the intramolecular distances and angles, the HCOOH position in the cell, and the Nb$_{12}$ configuration. The calculated vibrational frequencies are presented in Table 7. The first group includes intramolecular frequencies, which are too high to be active at the experimental temperature.[23,24] The other two groups include HCOOH librations and rotations inside the Nb$_{12}$ cluster and own vibrations of the cluster. These frequencies are comparable with the experimental temperature. According to the theory of radiationless transitions,[1,14,18] the argument of the tunneling rate constant as a function of temperature is $\hbar\omega_\alpha/4k_BT$. Here, k_B and $\hbar$ are the Boltzmann and Plank constants, respectively, T is the temperature, ω_α represents phonon frequencies. In our approximation, the values of ω_α are replaced by the Debye frequency ω_D or the frequency of a local mode of the HCOOH motion in the cluster.

So, the continuous phonon spectrum of the matrix and local vibrations of HCOOH contribute to the temperature dependence of the rate constant of intramolecular H-atom tunneling. The rate constant as a function of temperature is presented in the double adiabatic approximation[1,13−15] using the theory of ra-

diationless transitions[1,57,58] and accounting for the HCOOH local rearrangement and matrix reorganization. According to the theory,[1,14,16,20] at very low temperatures ($\hbar\omega_D(\omega') \gg 4k_BT$) the following expression for the rate constant of an exothermic process can be obtained:

$$k(T) = k_0 \exp\left\{ -\frac{E_r'}{\hbar\omega'} \tanh\left(\frac{\hbar\omega'}{4k_BT}\right) + \frac{7\pi^4}{90} \frac{E_r}{\hbar\omega_D}\left(\frac{k_BT}{\hbar\omega_D}\right)^4 \right\} \tag{2}$$

The terms in the exponent describe the influence on the temperature dependence of the rate constant of both local modes of the HCOOH motions in the Nb_{12} cluster (the first term) and the continuous spectrum of own vibrations of the Nb_{12} cluster (the second term). The external motion of HCOOH is considered here as a vibration with the effective frequency ω'. The corresponding reorganization energy is equal to E_r'. A continuous phonon spectrum is valid for describing the medium at considered temperatures, and E_r is the matrix reorganization energy for the Debye phonon spectrum.[16,35]

At higher temperatures ($\hbar\omega_D \sim 4k_BT$; ω' is arbitrary), in the range of classical intermolecular vibrations of the Nb_{12} cluster, the rate constant expression takes the form

$$k(T) = k_0' \exp\left\{ -\frac{E_r'}{\hbar\omega'} \tanh\left(\frac{\hbar\omega'}{4k_BT}\right) - \frac{(\Delta E - E_r)^2}{4E_r k_BT} \right\} \tag{3}$$

Here, ΔE is the defect of energy, which is defined as the energy difference between the initial and final positions of the H atom in potential wells, i.e., the difference between the energy of the cis ground vibrational state and the final energy of the trans state with possible excitation of some vibrational levels of the formic acid molecule. Similar to eq 2, the first term in the exponent describes the reorganization of the local mode, and the second one corresponds to the matrix reorganization. The expression for the last term coincides for the classical, Einstein, and Debye approximations describing the surrounding matrix.[12,14,16] The rate constant expressions for the classical and Einstein models of the medium[12−14] are known for a long time. The corresponding formula for the Debye model of solids was derived recently.[16] The pre-exponential factors k_0 and k_0', as usual, depend exponentially on the quasiclassical action of the tunneling particle under the barrier. Note that eqs 2 and 3 are also justified for intramolecular processes and charge transfer (electrons or protons) with local and media rearrangements. For example, similar rearrangements may occur with the impurities in solids between which a charge transfer takes place.

6. Comparison of Theory with the Experimental Data

Equations 2 and 3 are used in this section for fitting theoretical results to the experimental data[23,24] on intramolecular H-atom tunneling in the formic acid cis−trans conversion in solid Ar, Xe, and Kr. We emphasize that only temperature dependence of the rate constant will be considered here because of the peculiarities related to the accuracy of the potential barrier calculation (see the comment below eq 1). This accuracy is very important since the rate constant depends on the value of the potential barrier exponentially. This issue was discussed in detail earlier.[20] The weak temperature dependence of the pre-exponential factor k_0' in eq 3 is taken into account in the fitting procedure.

a. Choice of Fitting Parameters. It follows from eqs 2 and 3 that the rate constant is determined by the parameters ΔE, E_r', E_r, ω', and ω_D. Let us consider their properties and evaluate their magnitudes on the basis of the data in Tables 7 and 9. According to the quantum chemical calculations, the released energies are in different ranges for the Ar, Kr, and Xe matrixes (see the last line in Table 9). It is easy to see that these energies are significantly greater than the defect of energy ΔE. Therefore, a part of the released energy may be used for exciting some intramolecular formic acid vibrational modes in the final state. After penetration through the potential barrier, the particle has a zero velocity. Also, the HCOOH molecule is flat (C_s-symmetric) in the initial and final states, being in the same position inside the Nb_{12} cage. Therefore, mostly symmetric vibrations can be activated, for which variations of geometry parameters are sufficient to change the energy by an amount corresponding to several vibrational quanta. After the sub-barrier cis−trans conversion of HCOOH, the most significant variations involve the HCO and OCO bond angles (Table 5). However, the corresponding energy change is too low to activate the HCO vibration (Table 7), and the most suitable candidate for the activation following the cis−trans conversion of HCOOH is the OCO bending. In this case the released energy is sufficient to activate two vibrational quanta. It is worth noting that the difference between the released energy and the HCO frequency is small and, due to additional interactions with the surrounding matrix, the HCO vibration may be also activated in some cases. It should be also noticed that an even number of quanta of A″ vibrations can be excited during this transition, like in the case of Franck−Condon progressions. The probability of such excitations depends on the distortion of the corresponding A″ vibrational modes, i.e., on the frequency change upon the cis−trans isomerization. For example, the Franck−Condon factor for a 0−2 transition for a distorted normal mode, $I_{cis-trans}^2 = [(\omega\omega')^{1/2}(\omega' - \omega)^2]/(\omega + \omega')^3$ in the harmonic approximation, can be significant only if the frequency change is large. However, as seen in Table 7, the distortion of the A″ normal modes in HCOOH upon the cis−trans transformation is rather small and therefore their excitation probability is almost negligible, with the largest Franck−Condon factor for the excitation of two quanta of the HOCO torsion being below 0.01.

A rough estimation of the energy of the OCO second excitation level taking into account the anharmonicity of the vibrations gives the following approximate values of ΔE: Ar, 158−200 cm^{-1}; Kr, 57−126 cm^{-1}; Xe, 34−106 cm^{-1}. The calculated ranges of the reorganization energy E_r' related to the change of the HCOOH position in the Nb_{12} cluster are the following: Ar, 58−64 cm^{-1}; Kr, 56−68 cm^{-1}; Xe, 25−41 cm^{-1}. The proper ranges of E_r are Ar 40−62 cm^{-1}, Kr 13−30 cm^{-1}, and Xe 15−51 cm^{-1}. As to the frequency ω' of HCOOH librations and rotations in the Nb_{12} cluster, here it is reasonable to take the smallest values from Table 7, because the corresponding term in the exponents of eqs 2 and 3 with the smallest value of ω' depends on temperature most strongly. These values of ω' are equal to 94 cm^{-1} for Ar, 80 cm^{-1} for Kr, and 59 cm^{-1} for Xe. Finally, the magnitudes for ω_D are Ar 62 cm^{-1}, Kr 45 cm^{-1}, and Xe 39 cm^{-1}. These calculated values are reasonable enough and correspond to the experimental data. It is also necessary to take into account that the real phonon spectrum is much more complicated than the Debye spectrum. For example, the experimental spectra[59] show peaks at frequencies less than ω_D, and there are no such peaks in the Debye spectrum. So, the effective frequency ω(eff) will be used as a fitting parameter
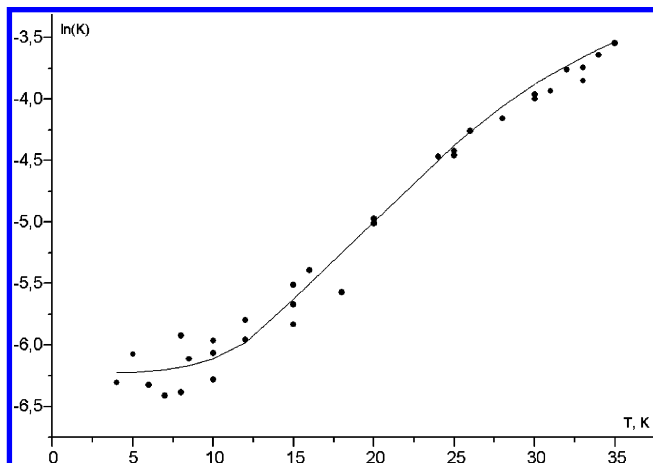
Figure 5. Temperature dependence of the rate constant of hydrogen tunneling in the cis to trans HCOOH conversion in the Ar matrix. The points are the experimental data (refs 23 and 24). The solid curve is the result of fitting of the theoretical temperature dependence (eqs 2 and 3) to the experimental data.
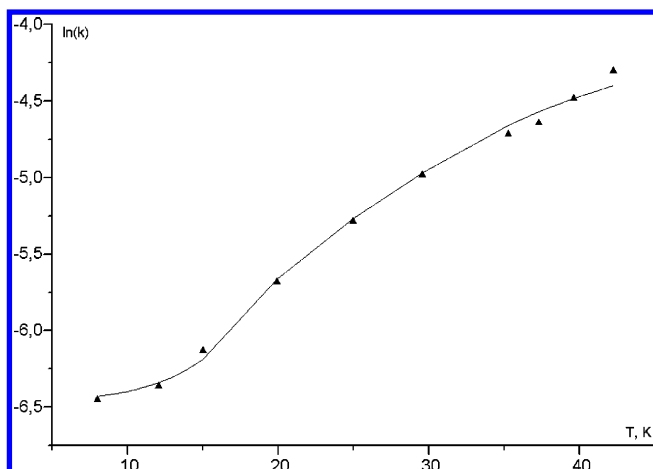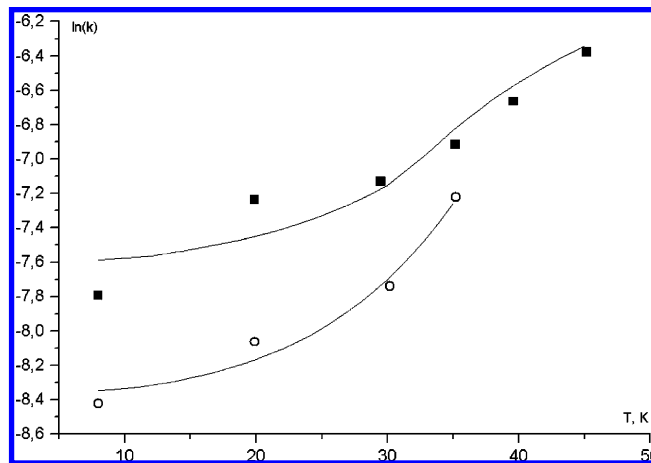

Figure 6. Temperature dependence of the rate constant of hydrogen tunneling in the cis to trans HCOOH conversion in the Kr matrix. The points are the experimental data (refs 23 and 24). The solid curve is the result of fitting the theoretical temperature dependence (eqs 2 and 3) to the experimental data.

instead of ω_D. Thus, three fitting parameters will be considered, ΔE, E_r, $\omega(\text{eff})$, and two fixed parameters, ω' and E_r'.

b. Fitting Procedure. As mentioned earlier, only temperature dependence of the rate constant is taken into account in the comparison of the experimental and theoretical data. At low temperatures, eq 2 is valid for the fitting and it is changed to eq 3 as the temperature increases. Then, both fitting curves have to match.

The fitting procedure gives for each matrix the curves plotted by eqs 2 and 3 with the fitted parameters a and b, so that the sum of squared deviations from the experimental points was minimal (see Figures 5−7). The values a and b are defined as

$$a = \frac{E_r}{\hbar\omega(\text{eff})}\left(\frac{k_B}{\hbar\omega(\text{eff})}\right)^4 \qquad b = (\Delta E - E_r)^2/4E_r k_B$$

$$(4)$$

These parameters correspond to the second terms in the exponents of eqs 2 and 3, respectively. The values of a and b can be obtained for the greater and smaller E_r' values. Then,

Figure 7. Temperature dependence of the rate constant of hydrogen tunneling in the cis to trans HCOOH conversion in the Xe matrix. The points are the experimental data (refs 23 and 24). The solid curve is the result of fitting of the theoretical temperature dependence (eqs 2 and 3) to the experimental data. The squares represent measurements in the Xe (1) matrix and circles are those for Xe (2).

the following steps are required to determine the fitting parameters ΔE, E_r, and $\omega(\text{eff})$.

1. For each pair a and b, the system of eqs 4 is solved with the greater and smaller quantum-chemically calculated values of E_r. This procedure gives allowable intervals for ΔE and $\omega(\text{eff})$.

2. By comparing these intervals for ΔE and $\omega(\text{eff})$ with quantum-chemically calculated intervals, one can find their intersections.

3. By substituting the greater and smaller values of ΔE intersection in eqs 4, we can determine the intervals for E_r and $\omega(\text{eff})$.

4. A comparison of these intervals with the quantum-chemical interval for E_r and values of $\omega(\text{eff})$ determined in step 2 allows us to find the appropriate intervals for all three fitting parameters.

5. The final step is to search intersections of the ΔE, E_r, and $\omega(\text{eff})$ intervals obtained for the greater and smaller values of E_r.

Below we present the fitted values of a and b corresponding to the greater $E_r'(\uparrow)$ and the smaller $E_r'(\downarrow)$:

Ar matrix: at $E_r'(\downarrow) = 58$ cm^{-1} these values are equal to $a_{Ar}(\downarrow) = 6.5 \times 10^{-6}$ cm^4, $b_{Ar}(\downarrow) = 56.5$ cm^{-1}, and at $E_r'(\uparrow) = 64$ cm^{-1} they are $a_{Ar}(\uparrow) = 6.6 \times 10^{-6}$ cm^4, $b_{Ar}(\uparrow) = 56.2$ cm^{-1}.

Kr matrix: at $E_r'(\downarrow) = 56$ cm^{-1} $a_{Kr}(\downarrow) = 2.6 \times 10^{-6}$ cm^4, $b_{Kr}(\downarrow) = 44.4$ cm^{-1}, and at $E_r'(\uparrow) = 68$ cm^{-1} $a_{Kr}(\uparrow) = 2.5 \times 10^{-6}$ cm^4, $b_{Kr}(\uparrow) = 42.0$ cm^{-1}.

In experiment,[24] there are two sets of data related to the Xe matrix. This is most likely related to slightly different conditions of matrix preparation.

Xe I matrix: at $E_r'(\downarrow) = 25$ cm^{-1} $a_{Xe\ I}(\downarrow) = 0.28 \times 10^{-6}$ cm^4, $b_{Xe\ I}(\downarrow) = 27$ cm^{-1}, and at $E_r'(\uparrow) = 41$ cm^{-1} $a_{Xe\ I}(\uparrow) = 0.21 \times 10^{-6}$ cm^4, $b_{Xe\ I}(\uparrow) = 28$ cm^{-1}.

Xe II matrix at $E_r'(\downarrow) = 25$ cm^{-1} $a_{Xe\ II}(\downarrow) = 0.29 \times 10^{-6}$ cm^4, $b_{Xe\ II}(\downarrow) = 27$ cm^{-1}, and at $E_r'(\uparrow) = 41$ cm^{-1} $a_{Xe\ II}(\uparrow) = 0.24 \times 10^{-6}$ cm^4, $b_{Xe\ II}(\uparrow) = 28$ cm^{-1}.

It is easy to see that, despite the experimental data differing significantly, the values of the parameters a and b for both Xe matrixes are very close.

c. Fitting Results and Discussion. The fitting parameters were calculated by following the procedure described in the

TABLE 10: Maximal Deviations of Theoretical Curves Describing Temperature Dependence of the Logarithm of the Tunneling Rate Constant from Experimental Curves

matrix	without change of parameters	10% change in ΔE	10% change in E_r	10% change in ω(eff)	combined 10% change in ΔE, E_r, ω(eff)
Ar	5%	29%	22%	7%	53%
Kr	3%	14%	10%	4%	26%
Xe	2%	9%	7%	3%	16%

previous subsection, and the following results were obtained using the fixed values of ω' and E_r' given above:

1. Ar matrix: $\Delta E = 158-180$ cm^{-1}, $E_r = 51-62$ cm^{-1}, ω(eff) $= 23.9-24.8$ cm^{-1}.

2. Kr matrix: $\Delta E = 61-101$ cm^{-1}, $E_r = 13-30$ cm^{-1}, ω(eff) $= 21.9-26.0$ cm^{-1}.

3. Xe I matrix: $\Delta E = 55-106$ cm^{-1}, $E_r = 15-40$ cm^{-1}, ω(eff) $= 35.1-42.8$ cm^{-1}.

4. Xe II matrix: $\Delta E = 55-106$ cm^{-1}, $E_r = 15-40$ cm^{-1}, ω(eff) $= 34.9-42.5$ cm^{-1}.

To better understand how well the fitting parameters are determined, we carried out their sensitivity analysis. With the values of the fitting parameters shown above, the maximal deviations of the theoretical curves describing temperature dependence of the logarithm of the tunneling rate constant from the corresponding experimental curves constituted 5%, 3%, and 2% for the Ar, Kr, and Xe I matrixes, respectively (see Table 10). A change of the ΔE value by 10% results in an increase of the maximal deviations to 29%, 14%, and 9% for Ar, Kr, and Xe I, respectively. If we change E_r by 10%, the maximal deviations grow respectively to 22%, 10%, and 7%. The 10% change in ω(eff) leads to an increase of the maximal deviations to 7%, 4%, and 3% for Ar, Kr, and Xe I, respectively. Finally, if all three fitting parameters ΔE, E_r, and ω(eff) are altered by 10% each, the maximal deviations are raised to 53%, 26%, and 16%, respectively, for the Ar, Kr, and Xe I matrixes. One can see that results are most sensitive with respect to the ΔE value and least sensitive with respect to ω(eff). Also, the sensitivity of the maximal deviations of the theoretical results from experiment decreases in the row Ar−Kr−Xe.

Consequently, the calculations demonstrate that all values of the fitted data are physically reasonable and lie within the intervals determined quantum chemically. As expected, the resulting fitting parameters for both Xe matrixes practically coincide. Only the effective frequencies of the matrix phonon spectrum slightly differ. Atomic bonds in the noble gas matrix are responsible for the phonon spectrum, but for each matrix they would be different. The ω(eff) values are substantially lower than the Debye frequencies for these crystals. A similar result was found earlier for D-atom tunneling in the HD crystal.[11,15,20] As mentioned above, such behavior of ω(eff) may be caused by the peculiarities of the real phonon spectrum of the sample, which differs significantly from the Debye spectrum.[59]

7. Conclusions

The temperature dependence of the rate constant of hydrogen intramolecular tunneling is studied here on the basis of the mechanism of the reagent and media reorganization upon an atom transfer proposed in earlier works.[32,33] The experimentally measured[23,24] cis−trans conversion of HCOOH embedded in Ar−Xe−Kr matrixes at extra low temperatures is considered. The parameters of the system, the height and width of the potential barrier of the reaction, the energy defect of the intramolecular subsystem, the energies of the reagent and media reorganization, and the frequencies of intermolecular vibrations are calculated quantum chemically by the MP2 method with extended basis sets. As shown in Table 9, the configurations of all matrixes change significantly as a result of intramolecular H-atom tunneling.

Expressions for the rate constant for intramolecular atom tunneling are derived for different temperature ranges. The fact that the temperature dependence of the reaction rate constant is determined by the matrix reorganization and the change of the HCOOH coordinates is taken into account. The matrix reorganization is described in the Debye approximation for the lattice motion and the formic acid vibrations in the cage are considered as an Einstein mode.

These theoretical expressions for the rate constant are compared with the experimental data[23,24] for the H-atom transfer. The computed values of energy reorganization of noble gas cages and HCOOH positions are used in the fitting procedure. The theory allows us to explain the experiment for the Ar−Xe−Kr matrixes[23,24] with reasonable values of the fitting parameters.

The developed method of the comparison of theoretical and experimental data can be used to study similar tunneling processes. Many similar monomolecular reactions can go through the analogous tunneling mechanism at low temperatures, and hence, the theoretical approach developed and tested here should provide a reliable foundation for the studies of such reactions and for substantiated comparison of theoretical and experimental data. Furthermore, the accuracy of theoretical predictions for the reorganization energy in such low-temperature tunneling systems can be substantially increased by employing quantum chemical calculations with larger model clusters.

References and Notes

(1) Goldanskii, V. I.; Trakhtenberg, L. I.; Fleurov, V. N. *Tunneling Phenomena in Chemical Physics*; Gordon and Breach Science Publishers: New York, NY, U.S., 1989.

(2) Benderskii, V. A.; Makarov, D. E.; Wight, C. A. *Chemical Dynamics at Low Temperatures*; Wiley: New York, NY, U.S., 1994.

(3) Miyazaki, T., Ed. *Atom Tunneling Phenomena in Physics, Chemistry and Biology*; Springer: Berlin, 2004.

(4) Trakhtenberg, L. I.; Klochikhin, V. L. *Chem. Phys.* **1998**, *232*, 175.

(5) Trakhtenberg, L. I.; Fokeyev, A. A.; Dolin, S. P.; Mebel, A. M.; Lin, S. H. *J. Chem. Phys.* **2005**, *123*, 114508.

(6) Hudson, R. L.; Shiotany, M.; Williams, F. *Chem. Phys. Lett.* **1977**, *48*, 193.

(7) Toriyama, K.; Nunome, K.; Iwasaki, M. *J. Am. Chem. Soc.* **1977**, *99*, 5823.

(8) Le Roy, R. J.; Murai, H.; Williams, F. *J. Am. Chem. Soc.* **1980**, *102*, 2325.

(9) Prass, B.; Colpa, J. P.; Stehlik, D. *J. Chem. Phys.* **1988**, *88*, 191.

(10) Prass, B.; Colpa, J. P.; Stehlik, D. *Chem. Phys.* **1989**, *136*, 187.

(11) Kumada, T.; Komaguchi, K.; Aratono, Y.; Miyazaki, T. *Chem. Phys. Lett.* **1996**, *261*, 463.

(12) Marcus, R. *J. Chem. Phys.* **1956**, *24*, 966; **1956**, *24*, 979; **1957**, *26*, 867.

(13) Dogonadze, R. R.; Kuznetsov, A. M. In *Proceedings of the Symposium on Electrocatalysis*; Breiter, M., Ed.; Princeton University Press: Princeton, NJ, U.S., 1974; p 195.

(14) Kuznetsov, A. M. *Charge Transfer in Physics, Chemistry and Biology*; Gordon and Breach: New York, NY, U.S., 1995.

(15) Ivanov, G. K.; Kozhushner, M. A.; Trakhtenberg, L. I. *J. Chem. Phys.* **2000**, *113*, 1992.

(16) Trakhtenberg, L. I.; Fokeyev, A. A. *J. Phys. Chem. A* **2007**, *111*, 9509.

(17) Klochikhin, V. L.; Pshezhetskii, S. Ya.; Trakhtenberg, L. I. *Dokl. Phys. Chem.* **1978**, *239*, 127.

(18) Trakhtenberg, L. I.; Klochikhin, V. L.; Pshezhetskii, S. Ya. *Chem. Phys.* **1982**, *69*, 121.

(19) Siebrand, W.; Smedarchina, Z.; Zgierski, M. Z.; Fernandes-Ramos, A. *Int. Rev. Phys. Chem.* **1999**, *18*, 5.

(20) Trakhtenberg, L. I. Theory of Atom Tunneling Reactions in Solid Phase. In *Atom Tunneling Phenomena in Physics, Chemistry and Biology*; Miyazaki, T., Ed.; Springer-Verlag: Heidelberg, Germany, 2004; pp 33−58.

(21) Grigoriev, E. I.; Trakhtenberg, L. I. *Radiation Chemical Processes in Solid Phase. Theory and Applications*, CRC Press Inc.: New York, London, Tokyo, 1996.

(22) Sekiya, H. Atom Tunneling and Molecular Structure. In *Atom Tunneling Phenomena in Physics, Chemistry and Biology*; Miyazaki, T., Ed.; Springer-Verlag: Heidelberg, Germany, 2004; pp 202−231.

(23) Pettersson, M.; Maçôas, E. M. S.; Khriachtchev, L.; Lundell, J.; Fausto, R.; Räsänen, M. *J. Chem. Phys.* **2002**, *117*, 9095.

(24) Marushkevich, K.; Khriachtchev, L.; Räsänen, M. *J. Chem. Phys.* **2007**, *126*, 241102.

(25) Bouldin, W. V.; Gordy, W. *Phys. Rev.* **1964**, *135*, 806.

(26) Grigoriev, E. I.; Pshezhetskii, S. Ya.; Trakhtenberg, L. I. *High Energy Chem.* **1985**, *19*, 41.

(27) Grigoriev, E. I.; Pshezhetskii, S. Ya.; Slavinskaya, N. A.; Trakhtenberg, L. I. *High Energy Chem.* **1987**, *21*, 519.

(28) Khriachtchev, L.; Lundell, J.; Isoniemi, E.; Räsänen, M. *J. Chem. Phys.* **2000**, *113*, 4265.

(29) Sander, S.; Willner, H.; Khriachtchev, L.; Pettersson, M.; Räsänen, M.; Varetti, E. L. *J. Mol. Spectrosc.* **2000**, *203*, 145.

(30) Brunton, G.; Griller, D.; Barclay, L. R. C.; Ingold, K. U. *J. Am. Chem. Soc.* **1976**, *98*, 6803.

(31) Brunton, G.; Gray, J. A.; Griller, D.; Barclay, L. R. C.; Ingold, K. U. *J. Am. Chem. Soc.* **1978**, *100*, 4197.

(32) Trakhtenberg, L. I. *Dokl. Phys. Chem.* **1983**, *269*, 1131.

(33) Trakhtenberg, L. I.; Slavinskaya, N. A.; Pshezhetskii, S. Ya. *Chem. Phys.* **1989**, *134*, 127.

(34) Trakhtenberg, L. I.; Fokeyev, A. A.; Zubin, A. S. *Russ. Chem. Bull.* **2008**, *6*, 1093.

(35) Trakhtenberg, L. I.; Fokeyev, A. A.; Zubin, A. S.; Mebel, A. M.; Lin, S. H. *J. Chem. Phys.* **2009**, *130*, 144502.

(36) Wawrzyniak, P. K.; Paneka, J.; Latajkaaa, Z.; Lundell, J. *J. Mol. Struct.* **2004**, *691*, 115.

(37) http://environmentalchemistry.com/yogi/periodic/Ar.html.

(38) http://environmentalchemistry.com/yogi/periodic/Kr.html.

(39) http://bizinfo.otrok.ru/chem/elem.php?n=54.

(40) Frisch, M. J.; Trucks, G. W.; Schlegel, H. B.; Scuseria, G. E.; Robb, M. A.; Cheeseman, J. R.; Montgomery, Jr., J. A.; Vreven, T.; Kudin, K. N.; Burant, J. C.; Millam, J. M.; Iyengar, S. S.; Tomasi, J.; Barone, V.; Mennucci, B.; Cossi, M.; Scalmani, G.; Rega, N.; Petersson, G. A.; Nakatsuji, H.; Hada, M.; Ehara, M.; Toyota, K.; Fukuda, R.; Hasegawa, J.; Ishida, M.; Nakajima, T.; Honda, Y.; Kitao, O.; Nakai, H.; Klene, M.; Li, X.; Knox, J. E.; Hratchian, H. P.; Cross, J. B.; Adamo, C.; Jaramillo, J.; Gomperts, R.; Stratmann, R. E.; Yazyev, O.; Austin, A. J.; Cammi, R.; Pomelli, C.; Ochterski, J. W.; Ayala, P. Y.; Morokuma, K.; Voth, G. A.; Salvador, P.; Dannenberg, J. J.; Zakrzewski, V. G.; Dapprich, S.; Daniels, A. D.; Strain, M. C.; Farkas, O.; Malick, D. K.; Rabuck, A. D.; Raghavachari, K.; Foresman, J. B.; Ortiz, J. V.; Cui, Q.; Baboul, A. G.; Clifford, S.; Cioslowski, J.; Stefanov, B. B.; Liu, G.; Liashenko, A.; Piskorz, P.; Komaromi, I.; Martin, R. L.; Fox, D. J.; Keith, T.; Al- Laham, M. A.; Peng, C. Y.; Nanayakkara, A.; Challacombe, M.; Gill, P. M. W.; Johnson, B.; Chen, W.; Wong, M. W.; Gonzalez, C.; Pople, J. A. *Gaussian 03*, Revision B.04; Gaussian, Inc.: Wallingford, CT, 2004.

(41) Woon, D. E.; Dunning, T. H., Jr. *J. Chem. Phys.* **1993**, *98*, 1358.

(42) Kendall, R. A.; Dunning, T. H., Jr.; Harrison, R. J. *J. Chem. Phys.* **1992**, *96*, 6796.

(43) Hay, P. J.; Wadt, W. R. *J. Chem. Phys.* **1985**, *82*, 270.

(44) Wadt, W. R.; Hay, P. J. *J. Chem. Phys.* **1985**, *82*, 284.

(45) Hay, P. J.; Wadt, W. R. *J. Chem. Phys.* **1985**, *82*, 299.

(46) Stevens, W.; Basch, H.; Krauss, J. *J. Chem. Phys.* **1984**, *81*, 6026.

(47) Stevens, W. J.; Krauss, M.; Basch, H.; Jasien, P. G. *Can. J. Chem.* **1992**, *70*, 612.

(48) Cundari, T. R.; Stevens, W. J. *J. Chem. Phys.* **1993**, *98*, 5555.

(49) Fuentealba, P.; Szentpaly, L. V.; Preuss, H.; Stoll, H. *J. Phys. B* **1985**, *18*, 1287.

(50) Igel-Mann, G.; Stoll, H.; Preuss, H. *Mol. Phys.* **1988**, *65*, 1321.

(51) Dolg, M.; Stoll, H.; Preuss, H. *J. Chem. Phys.* **1989**, *90*, 1730.

(52) Dolg, M.; Stoll, H.; Savin, A.; Preuss, H. *Theor. Chim. Acta* **1989**, *75*, 173.

(53) Kuechle, W.; Dolg, M.; Stoll, H.; Preuss, H. *Mol. Phys.* **1991**, *74*, 1245.

(54) Goddard, J. D.; Yamaguchi, Yu.; Schaefer, H. F., III. *J. Chem. Phys.* **1992**, *96*, 1158.

(55) Redington, R. L. *J. Mol. Spectrosc.* **1977**, *65*, 171.

(56) Bjamov, E.; Hocking, W. H. *Z. Naturforsch. Teil A* **1978**, *33*, 610.

(57) Kubo, R.; Toyozawa, Y. *Prog. Theor. Phys.* **1955**, *13*, 160.

(58) Kozhushner, M. A. In *Physico-Chemical Phenomena in Thin Films and at Solid Surfaces*; Trakhtenberg, L. I., Lin, S. H., Ilegbusi, O. J., Eds.; Elsevier Inc.: Amsterdam, 2007; pp 9−65.

(59) Ziman, J. M. *Principles of the Theory of Solids*; The University Press: Cambridge, U.K., 1972.